Facile Synthesis of Hierarchical ZnO:Tb3+ Nanorod Bundles and Their Optical and Magnetic Properties

ARTICLE *in* THE JOURNAL OF PHYSICAL CHEMISTRY C · FEBRUARY 2008

Impact Factor: 4.77 · DOI: 10.1021/jp710519q

4 AUTHORS, INCLUDING:

Lu Hong
Beihang University(BUAA)
189 PUBLICATIONS **2,740** CITATIONS
SEE PROFILE

Yexiang Tong
Sun Yat-Sen University
297 PUBLICATIONS **8,173** CITATIONS
SEE PROFILE

Facile Synthesis of Hierarchical ZnO:Tb^{3+} Nanorod Bundles and Their Optical and Magnetic Properties

Gao-Ren Li,*,†,‡ Xi-Hong Lu,† Cheng-Yong Su,† and Ye-Xiang Tong*,†

MOE of Key Laboratory of Bioinorganic and Synthetic Chemistry/School of Chemistry and Chemical Engineering/Institute of Optoelectronic and Functional Composite Materials, Sun Yat-Sen University, Guangzhou 510275, China, and State Key Lab of Rare Earth Materials Chemistry and Applications, Beijing 100871, China

Received: October 31, 2007; In Final Form: November 30, 2007

Here we explored a facile electrodeposition route to prepare large-area ZnO:Tb^{3+} nanorod bundles in a solution of $Zn(NO_3)_2$ + $Tb(NO_3)_3$ + CH_3COONH_4 at the temperature of 70 °C. The formation process of ZnO:Tb^{3+} nanorod bundles was investigated. When the concentration of CH_3COONH_4 was increased, the density of the nanorod bundles was largely increased, and the number of nanorod in the bundles also increased. The prepared ZnO:Tb^{3+} nanorod bundles were characterized by SEM, EDS, TEM, HRTEM, SAED, XRD, and XPS. According to the data of the absorption spectra, the optical band gaps (E_g) of ZnO:Tb^{3+} were estimated to be 3.13 eV. The luminescence of the prepared ZnO:Tb^{3+} nanorod bundles indicates these deposits have a high optical property. The magnetic measurements show the magnetic properties of ZnO:Tb^{3+} nanorod bundles are obviously affected by the temperature, and the blocking temperature is about 225 K, above which the deposits are superparamagnetic.

1. Introduction

Owing to a direct wide band gap (3.37 eV), large exciton binding energy (60 meV), and superior conducting properties based on oxygen vacancies, the wurtzite-structured ZnO has become one of the most promising materials for the fabrication of optoelectronic devices operating in the blue and UV region and the transparent conducting and piezoelectric materials for fabricating solar cells, electrodes, and sensors.[1−7] In order to design the electrical, optical, and magnetic properties of ZnO for the practicle applications, the control of shape and crystal structure are very important, and the synthesis of novel nanostructures is highly desired. For example, the preparation of various nanostructures, including nanorods, nanowires, nanotubes, nanobelts, and nanobranches, has been widely investigated.[8−14] However, it has been realized that tuning the band gap only by changing the morphology or size of nanocrystal is not well suited for some applications such as fluorescent imaging and nanoelectronics.[15−16]

It is well-known that the addition of impurities into a wide-band gap semiconductor can often induce dramatic changes in the optical, electrical, and magnetic properties.[17−18] Therefore, doping ZnO with a selective element has become an important route for enhancing and controlling its optical, electrical, and magnetic performance, which is usually crucial for their practical applications. The group III (B, Al, In, and Ga) and group IV (Pb and Sn) elements as the dopants are usually used to enhance the conductivities of ZnO.[4] Doping ZnO with magnetic ions, such as Co^{2+} and Mn^{2+}, as diluted magnetic semiconductors to impart the unusual giant Zeeman, Faraday rotation, and magnetic polaron effects.[19−20] Recently, much attention has been paid to adulterate ZnO with rare earth ions due to their unique optical, catalytic, and magnetic properties.[21−23] Of the many rare earth ions, the trivalent terbium ion (Tb^{3+}) is an important rare-earth dopant for green phosphors.[24−25] ZnO:Tb^{3+} nanostructures are assumed to be a new type of phosphor with interesting PL properties. However, the research of ZnO:Tb^{3+} nanostructures is still very limited. Here we first investigated the electrochemical deposition route for the preparation of ZnO:Tb^{3+} nanorod bundles. The growth rate, the surface morphology, and the composition can easily be well controlled by changing the electrodeposition parameters, such as, deposition potentials, current densities, and salt concentrations. The optical and magnetic properties of the prepared ZnO:Tb^{3+} nanorod bundles were also investigated.

2. Experimental Section

All electrochemical deposition experiments were performed with a Chi750B electrochemical workstation or a HDV-7C transistor potentiostatic apparatus connected to a three-electrode cell via galvanostatic electrolysis at 70 °C. The working electrodes were copper sheets (99.99 wt %) with areas of 0.8 cm^2. A graphite rod was used as the counter-electrode. A saturated calomel electrode (SCE) was used as the reference electrode that was connected to the cell with a double salt bridge system. All potential values determined in this study were the values versus SCE. The dehydrated $Tb(NO_3)_3$ was obtained by the reaction of Tb_2O_3 (99.99%) with HNO_3 and then dehydrating in vacuum at 353 K. The current densities of electrochemical deposition were chosen as 4.0∼5.0 mA/cm^2.

The surface morphologies of ZnO:Tb^{3+} deposits were observed with a field emission scanning electron microscope (JSM-6330F FE-SEM). Transmission electron microscopy (JEM-2010HR TEM) and electron diffraction (ED) were used to characterize the microstructures of the deposits. The deposits were also analyzed by X-ray energy dispersive spectroscopy

* To whom correspondence should be addressed. E-mail: ligaoren@mail.sysu.edu.cn (G.-R. Li); chedhx@mail.sysu.edu.cn (Y.-X. Tong).

† Sun Yat-Sen University.

‡ State Key Lab of Rare Earth Materials Chemistry and Applications.

10.1021/jp710519q CCC: $40.75
Published on Web 02/05/2008

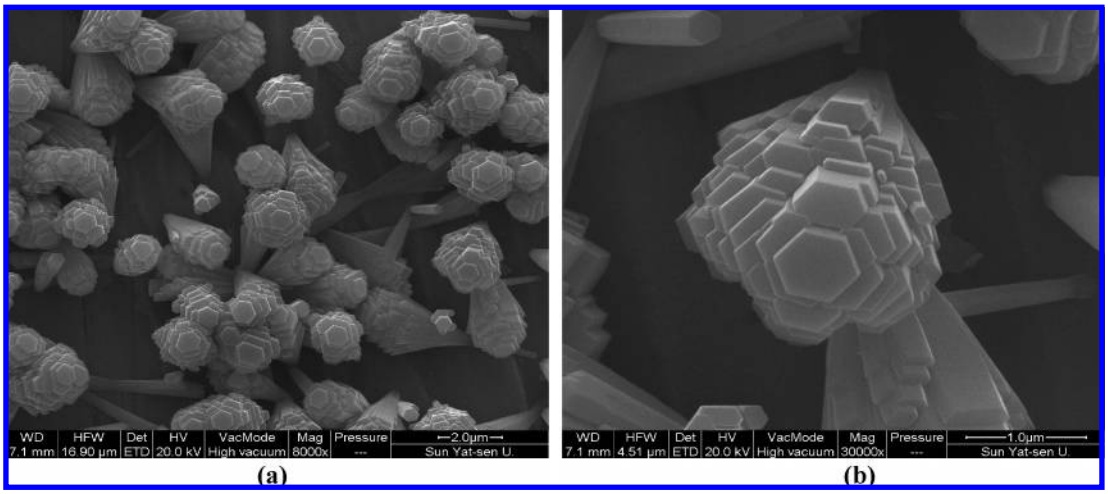

Figure 1. SEM images of ZnO:Tb^{3+} nanorod bundles prepared in solution of 0.01 M $Zn(NO_3)_2$+0.02 M $Tb(NO_3)_3$+0.2 M CH_3COONH_4 with current density of 2 mA/cm^2 for 2.5 h at 70 °C. (a) × 8, 000; (b) × 30, 000.

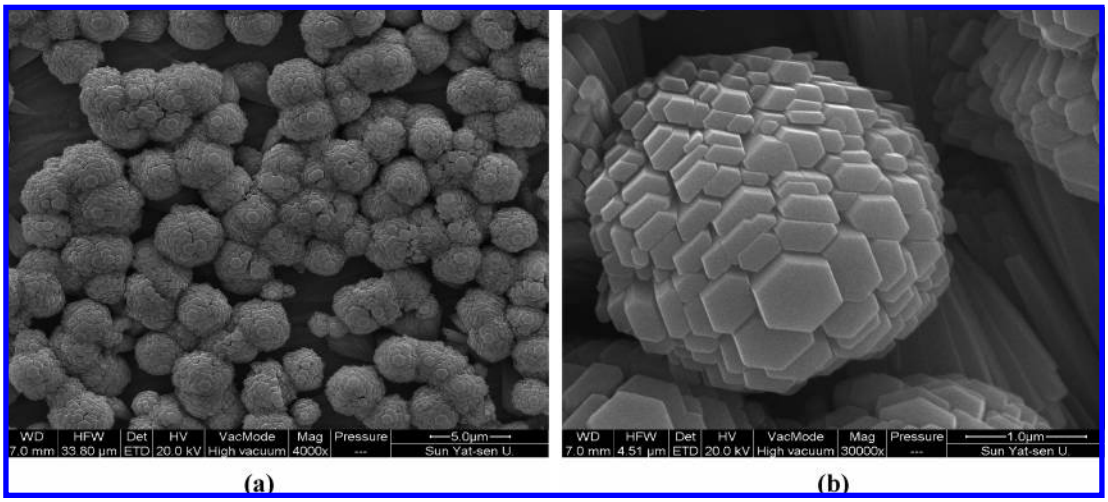

Figure 2. SEM images of ZnO:Tb^{3+} nanorod bundles prepared in solution of 0.01 M $Zn(NO_3)_2$+0.02 M $Tb(NO_3)_3$+0.05 M CH_3COONH_4 with current density of 2 mA/cm^2 for 2.5 h at 70 °C. (a) ×4, 000; (b) ×30, 000.

(EDS) to determine the contents of Tb, Zn, and O and by X-ray diffraction (XRD) to determine the structures. Photoluminescence (PL) spectra were carried out by spectrofluorophotometer (RF-5301PC) at room temperature. The absorption measurements were performed using a Shimadzu UV-3150 UV−vis−IR spectrometer at room temperature.

3. Results and Discussion

The electrodeposition of ZnO:Tb^{3+} was carried out in a solution of 0.01 M $Zn(NO_3)_2$ + 0.02 M $Tb(NO_3)_3$ + 0.2 M CH_3COONH_4 with a current density of 2mA/cm^2 for 2.5 h at 70 °C. The SEM images of the deposits were shown in Figure 1, and it clearly shows that the hierarchical ZnO:Tb^{3+} nanorod bundles were successfully obtained. In these nanorod bundles, a normal hexagonal microrod stands in the center and many quadrangular nanorods hierarchically stand around the central microrod. The size of the top of the nanorod bundles that is about 1.5∼2.0 μm is much larger than that of the bottom that is about 0.25 μm. The lengths of these nanorod bundles are about 4.0 μm. The central hexagonal microrod is highest, and the adjacent nanorods surrounding the central nanorod become lower gradually. The sizes of the central hexagonal microrod are about 500 nm, and those of the circumjacent quadrangular nanorods are about 200∼350 nm. When the concentration of CH_3COONH_4 was increased from 0.2 to 0.5 M, namely, the

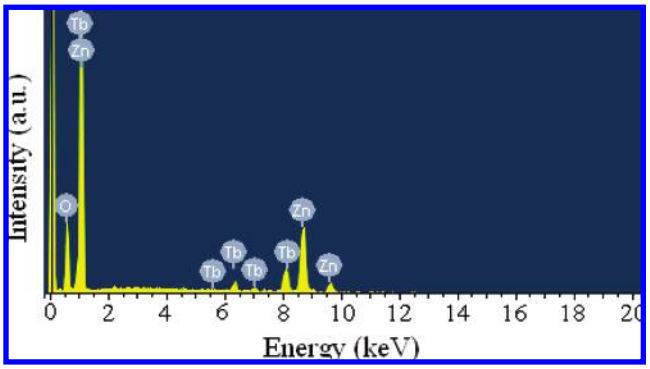

Figure 3. EDS spectrum of ZnO:Tb^{3+} nanorod bundles prepared in solution of 0.01 M $Zn(NO_3)_2$+0.02 M $Tb(NO_3)_3$+0.05 M CH_3COONH_4 with current density of 2 mA/cm^2 for 2.5 h at 70 °C.

electrochemical deposition was carried out in solution of 0.01 M $Zn(NO_3)_2$ + 0.02 M $Tb(NO_3)_3$ + 0.05 M CH_3COONH_4 with current density of 2 mA/cm^2 for 2.5 h at 70 °C, the hierarchical ZnO:Tb^{3+} nanorod bundles were also successfully prepared. The density of ZnO:Tb^{3+} nanorod bundles was largely increased as shown in Figure 2a. Furthermore, the number of nanorod in the bundles is also largely increased as shown in Figure 2b.

The EDS measurements were carried out at a number of locations throughout the single nanorod. Although taken from

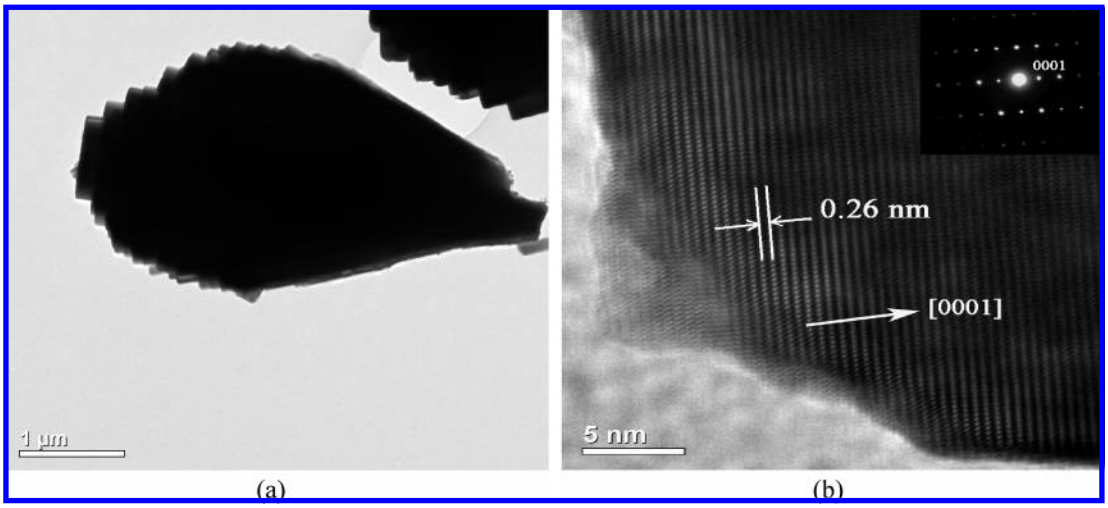

Figure 4. TEM image (a), HRTEM image (b), and SAED pattern (inset) of the prepared ZnO:Tb^{3+} nanorod bundles.

the different positions in the nanorod, we obtained the similar Tb doping with the same concentration. The representative EDS patterns were shown in Figure 3. The peaks of Tb were observed at about 1.0, 5.5, 6.2, 7.0, and 8.1 keV. An oxygen peak at about 0.5 keV and Zn signals at about 1.0, 8.6, and 9.6 keV could be observed, respectively. The EDS results revealed the prepared nanorod bundles were assuredly composed of Tb, Zn, and O. The concentration of Tb in the prepared deposit is about 6 atom %. The transmission electron microscopy (TEM) and high-resolution transmission electron microscopy (HRTEM) observations were carried out. The TEM image in Figure 4a further shows the obtained ZnO:Tb^{3+} deposits were hierarchical nanorod bundles. The HRTEM image for the prepared ZnO:Tb^{3+} nanorod bundles was shown in Figure 4b, which clearly shows that the lattice fringes derive from the same crystalline grains. The lattice spacing estimated from the HRTEM image was found to be around 0.26 nm, which corresponds to the (0002) planar spacing of ZnO in the wurtzite phase. So the crystal growth of the ZnO:Tb^{3+} nanorod bundles is preferential in the [0001] direction. The prepared ZnO:Tb^{3+} nanorod bundles was further characterized by the selected-area electron diffraction (SAED), and the SAED pattern in the inset in Figure 4b also shows that the prepared ZnO:Tb^{3+} nanorod bundles consists of single crystals with preferential growth in the [0001] direction. In addition, the HRTEM image and SAESD pattern were measured at a number of locations throughout the single nanorod, and the results are similar to that shown in Figure 4b, indicating Tb^{3+} possibly has been uniformly doped into wurtzite ZnO.

The XRD pattern was used to examine the crystal structure of the as-prepared ZnO:Tb^{3+} nanorod bundles, and Figure 5 shows the XRD pattern in the range of $2\theta = 10\sim80°$. Three peaks at about 31.8, 34.4, 36.2, 47.47, and 62.82° can be indexed to (100), (002), (101), (102), and (103) of wurtzite-structured ZnO (hexagonal phase, space group *P*63*mc*), the lattice constants ($a = 3.25$ Å, $c = 5.21$ Å) are in correspondence with the values in the standard card (JCPDS 36−1451). The stronger (002) diffraction peak in XRD pattern indicates that [0001] is the relatively preferred growth direction for ZnO:Tb^{3+} nanorod bundles. No any relational Tb crystalline forms are detected, which shows no phase separation existed in ZnO:Tb^{3+} nanorod bundles. This is accordant with the results of HRTEM and SAED. The incorporation of Tb^{3+} ions into the ZnO lattice and their vibration states were characterized by XPS measurement. The shift of the binding energy due to relative surface charging was corrected using the C 1s level at 284.6 eV as an internal

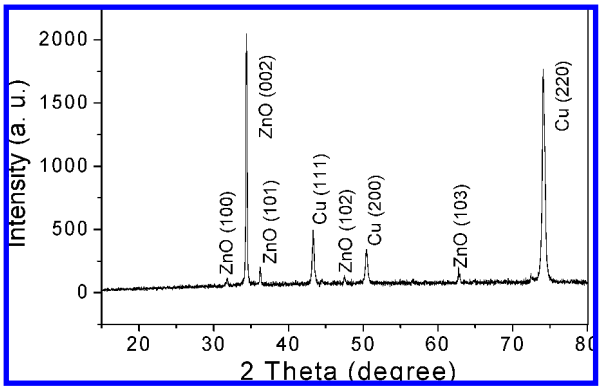

Figure 5. XRD pattern of the prepared ZnO:Tb^{3+} nanorod bundles.

standard. The fine XPS spectra of Zn $2p_{3/2}$ and O 1s are displayed in Figure 6a,b, respectively. The peaks located at 1021.4 and 1044.5 eV correspond to Zn $2p_{3/2}$ and Zn $2p_{1/2}$, respectively. The peak located at 530.3 eV corresponds to the electronic states of O 1s. The high-resolution scans of Tb $3d_{5/2}$ at 1242.4 eV and Tb $3d_{3/2}$ at 1276.7 eV are shown in Figure 6c. The high-resolution scan of Tb 4d was shown in Figure 6d, and it further demonstrated the existence of Tb^{3+} in deposit. Compared with standard XPS peak of Tb $3d_{5/2}$ at 1241.2 eV,[26] a slightly blueshift was observed for the peak of Tb $3d_{5/2}$ of the ZnO:Tb^{3+} deposits, which indicates that the distance between Tb and O in Tb_2O_3 has been changed because of the doping of Tb^{3+} ions. The quantitative analysis indicates that Tb^{3+} content in the obtained deposits is about 6.2 atom %. These obtained results of EDS, HRTEM, SAED, XRD, and XPS may reveal Tb^{3+} has been uniformly doped into wurtzite ZnO in principle. However, as the absence of an effective tool at present, the existence of the clusters of Tb in the deposits or not is very difficult to be well and truly judged and is still under investigated.

The formation process of ZnO:Tb^{3+} deposits was investigated here. When the electrodeposition was carried out, Tb^{3+} and Zn^{2+} ions will be transferred from bulk solution to cathode under the effect of electric field, and then they will obtain electrons on the surface of cathode to form Zn and Tb atoms. It is well-known that these newly formed Tb and Zn atoms are very active, and they will rapidly react with O_2 and H_2O in solution to form the oxides via reactions 1−4. Furthermore, the high-temperature (70 °C) can also promoted the corrosion of newly electro-reduced Zn and Tb atoms to form the stable passive phase ZnO and Tb_2O_3. In addition, the electro-reduction of the nitrate (NO_3^-

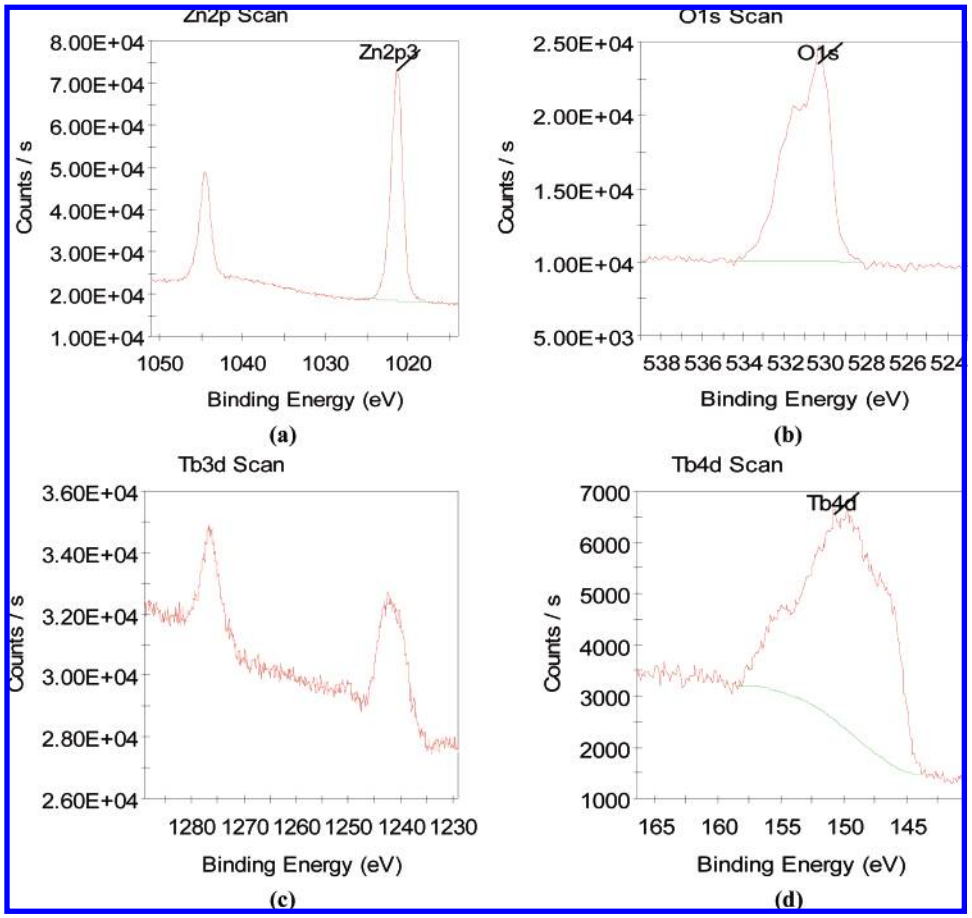

Figure 6. Fine XPS spectra of the prepared ZnO:Tb^{3+} nanorod bundles. (a): Zn region, (b): O region, (c): Tb 3d, and (d): Tb 4d region.

to NO_2^-) can produce OH^-, which will also result in the formation of ZnO and Tb_2O_3 via reactions 5−7. The produced ZnO and Tb_2O_3 will mix at molecular level, and Tb_2O_3 can uniformly enter into the crystal lattices of ZnO, which finally leads to the formation of ZnO:Tb^{3+}.

$$4Tb(s) + 3O_2(g) = 2Tb_2O_3(s) \quad (1)$$

$$2Zn(s) + O_2(g) = 2ZnO(s) \quad (2)$$

$$4Tb(s) + 6H_2O(l) = 2Tb_2O_3(s) + 3H_2(g) \quad (3)$$

$$Zn(s) + H_2O(l) = ZnO(s) + H_2(g) \quad (4)$$

$$NO_3^- + H_2O + 2e = NO_2^- + 2OH^- \quad (5)$$

$$Zn^{2+} + 2OH^- = ZnO + H_2O \quad (6)$$

$$2Tb^{3+} + 6OH^- = Tb_2O_3 + 3H_2O \quad (7)$$

During the electrodeposition, the isolated nuclei usually formed and randomly distributed on the substrate.[27−29] It is well-known that the surface of nuclei could adsorb some ions in deposition solution, such as NO_3^- and CH_3COO^-. These adsorbed NO_3^- or CH_3COO^- ions on the isolated ZnO:Tb^{3+} nuclei and the counterions, such as NH_4^+, may create an electrical double layer, which is responsible for generating a repulsive interaction between the isolated nuclei, affording electrostatic stabilization against aggregation.[30] In this study, the isolated nuclei finally evolve into the isolated nanorod bundles because of the growth of nuclei with deposition time increasing. In order to illustrate the growth process of nanorod bundles, a series of SEM images of ZnO nanorod bundles in various stages during the growth are shown in Figure 7a−c. It was observed the central nanorod was first formed as shown in Figure 7a, and then the outside nanorods subsequently formed. As the growth time of nanorods gradually decreased from the central to the outside, so the lengths and sizes of nanorods also gradually decreased. With deposition time increasing, the hierarchical nanorod bundles are finally formed. In addition, the densities of nanorods in the bundles are very high, and this causes many nanorods to form the anomalous hexagonal or quadrangular sections because of the space limit for the crystal growth of nanorods.

UV−vis spectrum of ZnO:Tb^{3+} nanorod bundles measured at room temperature were shown in Figure 8. According to the data for the absorption spectra, the optical band gaps (E_g) of ZnO:Tb^{3+} can be estimated by using the following equation:

$$\alpha h\upsilon = C(h\upsilon - E_g)^n$$

Here α is the absorption coefficient, $h\upsilon$ is photon energy, C is the constant. The band gaps of ZnO:Tb^{3+} can be estimated to be about 3.13 eV. The value of band gap of ZnO:Tb^{3+} is obviously smaller than that of bulk ZnO (3.37 eV). Considering the Bohr radius of ZnO is about 10 nm,[31] the quantum size effect is not expected from the above-mentioned nanostructures. It is well-known that the impurities introduced into ZnO nanostructures can modulate the local structure and cause the dramatic change of optical properties. Therefore, the red-shifted absorption onset from the prepared ZnO:Tb^{3+} nanostructures as compared with that of the bulk ZnO phase may be caused by the Tb^{3+} dopants. In addition, the absorbance peak of the

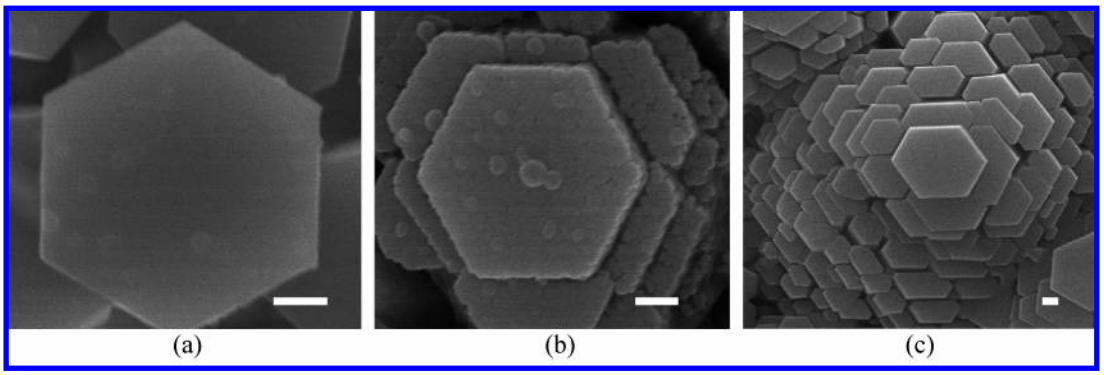

Figure 7. Illustration for the formation process of ZnO:Tb^{3+} nanorod bundles. The evolvement sequence is (a) → (b) → (c). (Scan bar is 100 nm).

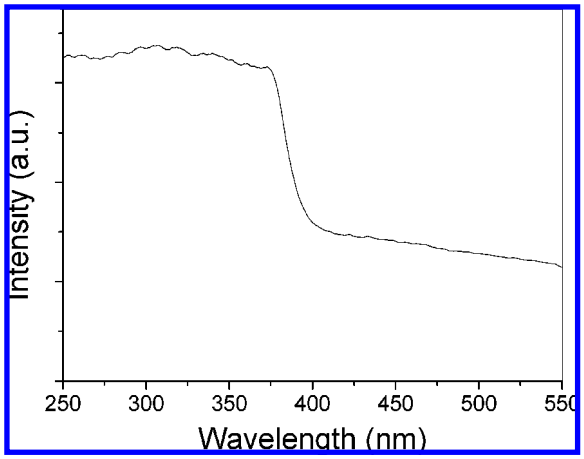

Figure 8. UV absorption spectrum of the prepared ZnO:Tb^{3+} nanorod bundles.

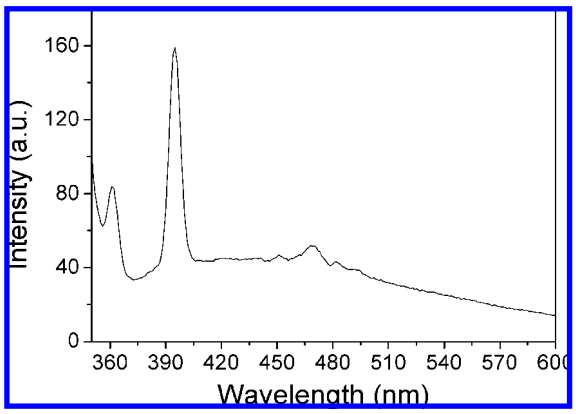

Figure 9. PL spectrum of the prepared ZnO:Tb^{3+} nanorod bundles.

UV−visible absorption spectrum becomes much broader with a lower energy shift, which gives a direct evidence for the decrease of band gap (E_g) and the energy broadening of valence band states attributable to the doping. As the doped elements enter the ZnO crystal lattices, the localized band edge states form at the doped sites with a reduction of E_g.

The PL spectra of the ZnO:Tb^{3+} nanorod bundles was shown Figure 9, and this spectra consist of two UV emission peaks centered at 361 and 394 nm, respectively, and a weak blue-green emission band centered at 469 nm. The result of the existence of two peaks at UV region is somewhat curious. It has been reported that two emission peaks centered at 390 nm (3.18 eV) and 395 nm (3.14 eV) were observed at UV region for ZnO epitaxial layers, and these two emission peaks were considered to originate from the different regions of the excitation area or at different intervals during excitation.[32] In addition, two UV peaks located at 378 nm (3.26 eV) and 387 nm (3.19 eV) were also observed for ZnO:Tb thin films on Si substrate grown by magnetron co-sputtering, and they were thought to be the recombination of free excitons through an exciton−exciton collision process and the excitonic recombination, respectively.[33] In our experiment, the UV emission band centered at about 394 nm corresponds to the near-band-edge emission.[34] The UV emission peak centered at 361 nm corresponds to the recombination of free excitons, which may be effected by the change of crystal structure of ZnO because of Tb^{3+} ions in ZnO crystal lattices, leading to a blue-shift of the emission peak. In the case of rare-earth-ion-doped semiconductors transfer of energy from the host to rare-earth ions often result in strong suppression and/or modification of the host luminescence.[36−39] In fact, such modification can be taken to be an evidence for energy transfer from the host to the rare earth ions. No UV emission related to the Tb^{3+} ion is observed, which is consistent with the previous results.[40] However, the Tb^{3+} ions have an important effect on the UV emission of ZnO. For bulk ZnO, it mainly exhibits a narrow emission peak near the band-edge free-exciton emission at about 390 nm and the full width at half-maximum (FWHM) of this UV emission is about 18 nm. However, for the ZnO:Tb^{3+} nanorod bundles, the FWHM of the UV emission at 394 nm is calculated to be about 8 nm. Therefore, the FWHM ZnO:Tb^{3+} nanorod bundles is much narrower than that of bulk ZnO crystals, and the obtained ZnO:Tb^{3+} nanorod bundles show a high optical property. Notice that a very weak green emission peak at 469 nm, originated from the intrinsic defect centers such as a zinc vacancy (V_{Zn}), interstitial zinc (Zn_i) or an oxygen vacancy (V_O), is present.

Magnetization curves of ZnO:Tb^{3+} nanorod bundles measured at 298 K were shown in Figure 10a, curves 1 and 2, respectively. The coercivity field (H_c) and the remanent magnetization (M_r) are almost zero at room temperature as shown in Figure 10a, and no hysteresis was observed. The magnetization nonlinearly increases with the applied field increasing, and it does not saturate even for the applied fields of 70 kOe. This behavior is in agreement with the magnetization curve of the superparamagnetic system. Such superparamagnetic behavior at room temperature is a common phenomenon for magnetic particles smaller than 20 nm. However, in this paper the ZnO:Tb^{3+} nanorod bundles all show the obvious superparamagnetic properties at 293 K, and this phenomenon can be attributed to the high anisotropy of the sample derived from both its structural features and the enhanced surface spin disorder.[41] However, the ZnO:Tb^{3+} nanorod bundles show distinct hysteresis loop at 5

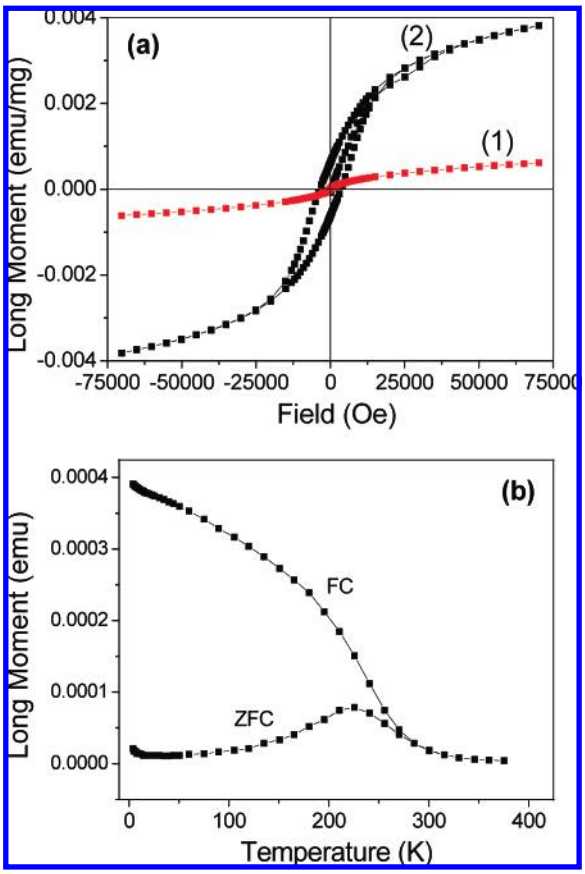

Figure 10. (a) Magnetization curves at (1) 293 K and (2) 5 K; (b) ZFC and FC magnetization curves of ZnO:Tb^{3+} nanorod bundles.

K as shown in Figure 10a, curve 2, indicating its ferromagnetic characteristic at 5 K. The H_c is about 3700 Oe, the M_r is about 6.67E-4 emu/mg, and the saturation magnetization (M_s) is about 0.04 emu/mg. The magnetic properties of ZnO:Tb^{3+} nanorod bundles are obviously affected by the temperature as shown in Figure 10a. The temperature dependence of the magnetization was measured, and by means of zero field-cooling (ZFC) and field-cooling (FC) analysis we can obtain the blocking temperature that is about 225 K (the maximum of the ZFC curve), above which the deposits are superparamagnetic (Figure 10b). As we all know, the appearance of ferromagnetism on the adulterated ZnO can be often attributed to the oxygen vacancy, clusters, secondary phases, and the fusion of defects at the interfaces.[42] In addition, the theoretical studies showed that the oxygen vacancies can alter the band structure of host oxides and make a great contribution to the ferromagnetism.[43] To exclude the effects of oxygen vacancies that are easily introduced during the electrodeposition growth process, the magnetic curve for the ZnO film containing no Tb^{3+} is depicted for reference, showing no ferromagnetism. The details for the magnetism of the prepared ZnO:Tb^{3+} nanorod bundles were still under investigated.

In summary, the ZnO:Tb^{3+} nanorod bundles could be successfully synthesized by electrochemical deposition, which represents a simple, quick, and economical method. The results of XRD, EDS, XPS, HRTEM, and SAED primarily revealed that the prepared ZnO:Tb^{3+} deposits are composed of single-crystal structures with preferential growth in the (0001) direction without any phase separation. The result of the UV−vis spectrum shows that the value of band gap of ZnO:Tb^{3+} is obviously smaller than that of bulk ZnO. The Tb^{3+} ions have an important effect on the UV emission of ZnO. In addition, ZnO:Tb^{3+} nanorod bundles show ferromagnetic characteristic at 5 K. The direct electrochemical synthetic method represents a considerable improvement for the preparation of adulterated ZnO samples because of allowing better control over the dopant and their nanostructures, and may therefore provide a better experimental basis for understanding and ultimately controlling the optical and magnetic properties of this class of materials.

Acknowledgment. This work was supported by the Natural Science Foundations of China (Grant Nos. 20603048 and 20573136), the Natural Science Foundations of Guangdong Province (Grant Nos. 06300070, 06023099, and 04205405), and the Foundations of Potentially Important Natural Science Research and Young Teacher Starting-up Research of Sun Yat-Sen University.

Note Added after ASAP Publication. This article was published ASAP on February 5, 2008. The caption to Figure 6 has been modified. The correct version was published on February 12, 2008.

References and Notes

(1) Huang, M. H.; Mao, S.; Feick, H.; Yan, H.; Wu, Y.; Kind, H.; Weber, E.; Russo, R.; Yang, P. *Science* **2001**, *292*, 1897.
(2) Pan, Z. W.; Dai, Z. R.; Wang, Z. L. *Science* **2001**, *291*, 1947.
(3) Shen, G.; Cho, J. H.; Yoo, J. K.; Yi, G.-C.; Lee, C. J. *J. Phys. Chem. B* **2005**, *109*, 5491−5496.
(4) Xu, L.; Su, Y.; Chen, Y.; Xiao, H.; Zhu, L.; Zhou, Q.; Li, S. *J. Phys. Chem. B* **2006**, *110*, 6637−6642.
(5) Dong, L. F.; Cui, Z. L.; Zhang, Z. K. *Nanostruct. Mater.* **1997**, *8*, 815.
(6) Rau, U.; Schmidt, N. *Thin Solid Films* **2001**, *387*, 141.
(7) He, J. H.; Lao, C. S.; Chen, L. J.; Davidovic, D.; Wang, Z. L. *J. Am. Chem. Soc.* **2005**, *127*, 16376−16377.
(8) Liao, L.; Lu, H. B.; Li, J. C.; He, H.; Wang, D. F.; Fu, D. J.; Liu, C.; Zhang, W. F. *J. Phys. Chem. C* **2007**, *111*, 1900−1903.
(9) Liu, T.-Y.; Liao, H.-C.; Lin, C.-C.; Hu, S.-H.; Chen, S.-Y. *Langmuir* **2006**, *22*, 5804−5809.
(10) Shan, C. X.; Liu, Z.; Zhang, Z. Z.; Shen, D. Z.; Hark, S. K. *J. Phys. Chem. B* **2006**, *110*, 11176−11179.
(11) Li, L.; Pan, S.; Dou, X.; Zhu, Y.; Huang, X.; Yang, Y.; Li, G.; Zhang, L. *J. Phys. Chem. C* **2007**, *111*, 7288−7291.
(12) Tong, Y.; Liu, Y.; Shao, C.; Liu, Y.; Xu, C.; Zhang, J.; Lu, Y.; Shen, D.; Fan, X. *J. Phys. Chem. B* **2006**, *110*, 14714−14718.
(13) Wang, X.; Ding, Y.; Summers, C. J.; Wang, Z. L. *J. Phys. Chem. B* **2004**, *108*, 8773−8777.
(14) Li, G.-R.; Lu, X.-H.; Qu, D.-L.; Yao, C.-Z.; Zheng, F.-l.; Bu, Q.; Dawa, C.-R.; Tong, Y.-X. *J. Phys. Chem. C* **2007**, *111*, 6678−6683.
(15) Bailey, R. E.; Nie, S. *J. Am. Chem. Soc.* **2003**, *125*, 7100.
(16) Wang, Y. S.; Thomas, P. J.; O'Brien, P. *J. Phys. Chem. B* **2006**, *110*, 21412−21415.
(17) Sanon, G.; Rup, R.; Mansingh, A. *Phys. Rev. B* **1991**, *44*, 5672.
(18) Sernelius, B. E.; Berggren, K. F.; Jin, Z. C.; Hamber, I.; Granqvist, C. G. *Phys. Rev. B* **1998**, *37*, 10244.
(19) *Semiconductors and Semimetals*; Willardson, R. K., Beer, A. C., Eds.; *Diluted Magnetic Semiconductors*; Furdyna, J. K., Kossut, J., Eds.; Vol. 25; Academic: New York, 1988.
(20) Radovanovic, P. V.; Norberg, N. S.; McNally, K. E.; Gamelin, D. R. *J. Am. Chem. Soc.* **2002**, *124*, 15192−15193.
(21) Teng, X. M.; Fan, H. T.; Pan, S. S.; Ye, C.; Li, G. H. *J. Appl. Phys.* **2006**, *100*, 053507.
(22) John, J. S.; Coffer, J. L. *Appl. Phys. Lett.* **2000**, *77*, 1635−1637.
(23) Komuro, S.; Katsumata, T.; Morikawa, T. *Appl. Phys. Lett.* **2000**, *76*, 3935−3937.
(24) Lin, J.; Huang, Y.; Zhang, J.; Gao, J.; Ding, X.; Huang, Z.; Tang, C. *Chem. Mater.* **2007**, *19*, 2585- 2588.
(25) Guo, C. X.; Zhang, W. P.; Shi, C. S. *J. Lumin.* **1981**, *24-25* (Part 1), 297.
(26) Paladia, D.; Lang, W. C.; Norris, P. R.; Watson, L. M.; Fabian, P. J. *Proc. R. Soc. London, Ser. A* **1977**, *354*, 269.
(27) Radisic, A.; Ross, F. M.; Searson, P. C. *J. Phys. Chem. B* **2006**, *110*, 7862−7868.

(28) Radisic, A.; Vereecken, P. M.; Searson, P. C.; Ross, F. M. *Surf. Sci.* **2006**, *660*, 1817−1826.
(29) Zoval, J. V.; Stiger, R. M.; Biernacki, P. R.; Penner, R. M. *J. Phys. Chem.* **1996**, *100*, 837−844.
(30) Ng, C. H. B.; Fan, W. Y. *J. Phys. Chem. B* **2006**, *110*, 20801−20807.
(31) Kar, S.; Dev, A.; Chaudhuri, S. *J. Phys. Chem. B* **2006**, *110*, 17848−17853.
(32) Bagnall, D. M.; Chen, Y. F.; Zhu, Z.; Yao, T.; Shen, M. Y.; Goto, T. *Appl. Phys. Lett.* **1998**, *73*, 1038.
(33) Kim, M.-J.; Mebratu, G. K.; Sung, J.-Y.; Shin, J. *J. Non-Cryst. Solids* **2003**, *315*, 312.
(34) Li, C.; Fang, G.; Su, F.; Li, G.; Wu, X.; Zhao, X. *Cryst. Growth Des.* **2006**, *6*, 2589.
(35) Teng, X. M.; Fan, H. T.; Pan, S. S.; Ye, C.; Li, G. H. *J. Appl. Phys.* **2006**, *100*, 053507.
(36) Fujii, M.; Yoshida, M.; Kanzawa, Y.; Hayashi, S.; Yamamoto, K. *Appl. Phys. Lett.* **1997**, *71*, 1298.
(37) Kik, P. G.; Polman, A. *J. Appl. Phys.* **2000**, *88*, 1992.
(38) Kuhne, H.; Weiser, G. *J. Appl. Phys.* **1996**, *86*, 896.
(39) Seo, S.-Y.; Shin, H. *Appl. Phys. Lett.* **2004**, *84*, 4379.
(40) Liu, S. M.; Liu, F. Q.; Guo, H. Q.; Zhang, Z. H.; Wang, Z. G. *Phys. Lett. A* **2000**, *271*, 128.
(41) Crisan, O.; Angelakeris, M.; Simeonidis, K.; Kehagias, T.; Komninou, P.; Giersig, M.; Flevaris, N. K. *Acta Mater.* **2006**, *54*, 5251−5260.
(42) Jayakumar, O. D.; Gopalakrishnan, I. K.; Kulshreshtha, S. K. *Adv. Mater.* **2006**, *18*, 1857.
(43) Jaffe, J. E.; Droubay, T. C.; Chambers, S. A. *J. Appl. Phys.* **2005**, *97*, 0733908.